HHS Public Access

Author manuscript

Nat Med. Author manuscript; available in PMC 2019 January 23.

Published in final edited form as:

Nat Med. 2018 August ; 24(8): 1143–1150. doi:10.1038/s41591-018-0116-5.

Tumor innate immunity primed by specific interferon-stimulated endogenous retroviruses

Israel Cañadas[1], **Rohit Thummalapalli**[1,*], **Jong Wook Kim**[1,2,*], **Shunsuke Kitajima**[1], **Russell William Jenkins**[1,3], **Camilla Laulund Christensen**[1], **Marco Campisi**[1], **Yanan Kuang**[4], **Yanxi Zhang**[1], **Evisa Gjini**[5], **Gao Zhang**[6], **Tian Tian**[7], **Debattama Rai Sen**[8], **Diana Miao**[1,2], **Yu Imamura**[9,10], **Tran Thai**[1], **Brandon Piel**[1], **Hideki Terai**[1], **Amir Reza Aref**[4], **Timothy Hagan**[11], **Shohei Koyama**[12], **Masayuki Watanabe**[9], **Hideo Baba**[10], **Anika Elise Adeni**[1], **Christine Anne Lydon**[1], **Pablo Tamayo**[13], **Zhi Wei**[7], **Meenhard Herlyn**[6], **Thanh Uyen Barbie**[1,14], **Ravindra Uppaluri**[1,14], **Lynnette Marie Sholl**[5], **Ewa Sicinska**[11], **Jacob Sands**[1], **Scott Rodig**[5], **Kwok Kin Wong**[1,15], **Cloud Peter Paweletz**[4], **Hideo Watanabe**[16,17], and **David Allen Barbie**[1]

[1]Department of Medical Oncology, Dana-Farber Cancer Institute, Boston, MA 02215, USA

[2]Broad Institute of Harvard and MIT, Cambridge, MA 02142, USA

[3]Division of Medical Oncology, Massachusetts General Hospital Cancer Center, Harvard Medical School, Boston, MA 02114, USA

[4]Belfer Institute for Applied Cancer Science, Dana Farber Cancer Institute, Boston, MA 02215, USA

[5]Department of Pathology, Brigham and Women's Hospital, Boston, MA 02115, USA

[6]Melanoma Research Center and Molecular and Cellular Oncogenesis Program, The Wistar Institute, Philadelphia, PA 19104 USA

[7]Department of Computer Science, New Jersey Institute of Technology, University Heights Newark, NJ 07102 USA

[8]Department of Pediatric Oncology, Dana-Farber Cancer Institute, Boston, MA 02115, USA

[9]Gastroenterological Surgery, The Cancer Institute Hospital of Japanese Foundation for Cancer Research 3-8-31, Ariake, Koto, Tokyo, 135-8550, Japan

Corresponding author: David A. Barbie, 450 Brookline Ave, LC4115, Boston, MA 02215. dbarbie@partners.org, Phone: (617) 632-6049, Fax: (617) 632-5786.

*These authors contributed equally to this work.

Author contributions

I.C and D.A.B designed research and wrote the manuscript. J.W.K., G.Z., T.Ti., D.M., P.T., Z.W., M.H. and H.W. performed and supervised computational analyses. I.C., R.T., S.Ki., R.W.J., M.C., T.Th., B.P., H.T., A.R.A., S.Ko., T.U.B., R.U., K.K.W. and D.A.B. performed and supervised biological and cellular studies. C.L.C., Y.I., T.H., M.W., H.B., A.E.A, C.A.L., L.M.S, E.S., and J.S. obtained samples, performed or supervised immunohistochemistry. E.G. and S.R. performed and supervised multiplexed immunofluorescence. D.R.S. and H.W. performed ATAC sequencing and analysis. C.L.C. and Y.Z. performed *in vivo* experiments. C.P.P and Y.K performed ddPCR experiments.

Competing Financial Interest Statement

D.A.B. is a consultant for N-of-One.

[10]Department of Gastroenterological Surgery, Graduate school of medical Sciences, Kumamoto University 1-1-1 Honjo, Chuo-ku, Kumamoto-city, Kumamoto, 860-8556, Japan

[11]Department of Oncologic Pathology, Dana-Farber Cancer Institute, Boston, MA 02215, USA

[12]Department of Respiratory Medicine, Allergy and Rheumatic Diseases, Osaka University Graduate School of Medicine, Japan

[13]Moores Cancer Center and School of Medicine, University of California San Diego, La Jolla, CA 92093, USA

[14]Department of Surgery, Brigham and Women's Hospital, Boston, MA 02115, USA

[15]Perlmutter Cancer Center, New York University (NYU) Langone Medical Center, New York, NY 10016, USA

[16]Department of Medicine, Division of Pulmonary, Critical Care and Sleep Medicine

[17]Tisch Cancer Institute, Icahn School of Medicine at Mount Sinai, New York, NY 10029, USA

Abstract

Mesenchymal tumor subpopulations secrete pro-tumorigenic cytokines and promote treatment resistance[1–4]. This phenomenon has been implicated in chemorefractory small cell lung cancer (SCLC) and resistance to targeted therapies[5–8], but remains incompletely defined. Here we identify a subclass of endogenous retroviruses (ERVs) that engages innate immune signaling in these cells. Stimulated 3 Prime Antisense Retroviral Coding Sequences (SPARCS) are oriented inversely in 3′UTRs of specific genes enriched for regulation by STAT1 and EZH2. De-repression of these loci results in dsRNA generation following IFNγ exposure due to bi-directional transcription from the STAT1-activated gene promoter and the 5′ LTR of the antisense ERV. Engagement of MAVS and STING activates downstream TBK1, IRF3, and STAT1 signaling, sustaining a positive feedback loop. SPARCS induction in human tumors is tightly associated with MHC class 1 expression, mesenchymal markers, and downregulation of chromatin modifying enzymes, including EZH2. Analysis of cell lines with high inducible SPARCS expression reveals strong association with an AXL/MET positive mesenchymal cell state. While SPARCS high tumors are immune infiltrated, they also exhibit multiple features of an immune suppressed microenviroment. Together, these data unveil a subclass of ERVs whose de-repression triggers pathologic innate immune signaling in cancer, with important implications for cancer immunotherapy.

Resistant SCLC undergoes a mesenchymal state switch induced by RAS/MET signaling or chemotherapy (e.g. H69M or H69AR subpopulations derived from H69 cell line) (Supplementary Fig. 1a)[9,10]. We noted enhanced innate immune and RAS signaling in H69M cells, including elevated phosphorylated-TBK1 (pTBK1), pIRF3, IKKε and NF-κB gene sets, and multiple secreted cytokines/chemokines (Figs. 1a,b and Supplementary Fig. 1b,c). TBK1 activity was preferentially increased in additional mesenchymal SCLC cell lines (Supplementary Fig. 1d, e), and subpopulations of human and murine $Rb^{L/L}/p53^{L/L}$ SCLC tumors (Fig. 1c and Supplementary Fig. 1f–h). Because H69M cells also attracted T cells and monocytes (Supplementary Fig. 2a–e), we explored immune checkpoint activation.

This identified a PD-L1^{high}, CD44^{high} fibroblastic subpopulation responsible for pTBK1 and cytokine/chemokine production (Fig. 1d–f and Supplementary Fig. 3a, b).

H69M PD-L1^{high} cells reverted phenotypically in culture and were genomically similar to parental H69 cells (Supplementary Fig. 3c, d), suggesting an epigenetic mechanism of innate immune activation. Since endogenous retroviruses (ERVs) undergo epigenetic silencing, we examined expression of a recently described ERV panel[11,12]. H69M-PD-L1^{high} cells exhibited marked upregulation of *MLT1C49* (Fig. 1g), an ERV poised to generate dsRNA due to antisense orientation in the 3′UTR of *TRIM22*, a STAT1 target gene[13]. Transfection of a 3′UTR construct containing this antisense ERV was sufficient to induce cytokine and *PD-L1* expression in H69M-PD-L1^{low} cells (Fig. 1h and Supplementary Fig. 4a, b), and in 293T cells (Supplementary Fig 4c). Conversely, siRNA mediated knockdown of *MLT1C49* partially inhibited *CXCL10* and *CCL2* expression in H69M-PD-L1^{high} cells (Fig. 1i and Supplementary Fig. 4d), validating a direct role in this innate immune phenotype, but suggestive of redundancy.

We therefore intersected all antisense 3′UTR ERVs from Ref Seq with H69M upregulated genes (Supplementary Dataset 1)[9], to identify additional ERV family members in this mesenchymal state with this unique genomic feature. This analysis identified *TRIM22/MLT1C49* and 14 other genes/ERVs including *TRIM38* which contained two (*MLT1J*, *MLT1A*), the majority of which were specifically induced in H69M-PD-L1^{high} cells (Fig. 1j and Supplementary Fig. 5a). Similar to TRIM22, many of these genes contained STAT1 motifs and/or binding sites[13,14] in their promoters (Supplementary Fig. 5b), which suggested inducibility by the IFNγ or other STAT1-activating factors already present in H69M conditioned media (Fig. 1b, f). Indeed, in contrast to H69 cells IFNγ stimulation of the additional mesenchymal subpopulation, H69AR, induced expression of most, but not all of these genes/ERVs, (Supplementary Fig 5c) validating a role for STAT1 mediated regulation. Conversely, IL32/THE1D and F3/MLT1I were inducible by IFNγ in H69AR cells, but not upregulated in H69M-PD-L1^{high} cells (Fig. 1j and Supplementary Fig. 5a, c), suggesting some differences in transcriptional state between mesenchymal subclones. Regardless, these studies uncovered a wider set of genes with 3′ antisense ERVs preferentially expressed in the mesenchymal cell state and regulated by STAT1 signaling. Because of the unique ability of interferons to trigger their expression, create dsRNA via bidirectional transcription, and spark feed-forward innate immune signaling, we term these ERVs Stimulated 3 Prime Antisense Retroviral Coding Sequences (SPARCS).

ERV dsRNAs are sensed by the RIG-1/MDA5-MAVS signaling pathway or reverse-transcribed and detected via the cGAS-cGAMP STING pathway[15]. Indeed, we observed STING upregulation and increased cytoplasmic *MLT1C49* dsDNA in H69M PD-L1^{high} cells (Supplementary Fig. 5d–f). *MAVS* or combined *MAVS*/*STING* deletion in H69M cells strongly impaired TBK1 and IRF3 phosphorylation (Fig. 1k), decreased multiple cytokines/chemokines, including CXCL10, CCL5, and CCL2 (Fig. 1l, m) and suppressed T cell and monocyte attraction (Supplementary Fig. 6a, b). Deletion of *MAVS* and/or *STING* also reverted the mesenchymal phenotype, increasing E-cadherin and decreasing Vimentin expression (Fig. 1k and Supplementary Fig. 6c,d). Thus, ERV sensing of SPARCS directly contributes to this cellular state.

IFNγ also induced robust PD-L1 expression in H69AR cells, suggesting that differential chromatin accessibility could underlie this responsiveness (Fig. 2a). Indeed, even a 10 min IFNγ pulse in H69AR, but not H69 cells, resulted in marked induction of *TRIM22* and *MLT1C49*, correlating with *PD-L1* mRNA and cytokine/chemokine secretion (Fig. 2b, c and Supplementary Fig. 7a, b). H69AR cells showed specific gain of chromatin accessibility around SPARCS loci, but not *PD-L1, CXCL10* or *CCL2* (Fig. 2d and Supplementary Fig. 7c). Because H69M and H69AR cells downregulated EZH2[16] (Fig. 2e), we examined whether EZH2 is involved in silencing SPARCS. EZH2 inhibitor treatment of H69 cells over 6 days enhanced similar IFNγ induced cytokines (Fig. 2f), and de-repressed the same SPARCS as in H69AR cells (Fig. 2g and Supplementary Fig. 7d). Thus, SPARCS loci are normally silenced and protected from IFN-induced expression by EZH2, but de-repressed in mesenchymal H69 subpopulations.

We next wondered if SPARCS promote positive feedback signal amplification. We detected high levels of dsRNA preferentially produced from *MLT1C49, MLT1J* and *MLT1A* in 10 min IFNγ pulsed H69AR cells, even after 24 h (Fig. 2h). TAG-aided sense/antisense transcript detection (TASA-TD) PCR[17] confirmed that dsRNA resulted from bidirectional transcription of *MLT1C49*, *MLT1J*, and *MLT1A* (Supplementary Fig. 8a). IFNγ pulse treatment activated and sustained pTBK1 and pIRF3 in addition to pSTAT1 in H69AR but not H69 cells (Fig. 2i), which further amplified SPARCS expression, pTBK1, and its effector cytokines over time (Fig. 2j and Supplementary Fig. 8b, c). Transfection of the dsRNA mimic Poly(I:C) induced type I/II IFNs in H69AR cells (Supplementary Fig. 8d) and direct IFNα/β exposure or Poly(I:C) itself induced SPARCS (Supplementary Fig. 8d, e), consistent with positive feedback induced by dsRNA and type I IFN. Furthermore, exposure of untreated H69AR cells to IFNγ primed conditioned medium activated TBK1 and STAT1 and induced *CXCL10*, *IFNβ* and ERV expression (Supplementary Fig. 9a–d). These data confirmed feedforward signaling downstream of SPARCS activation (Supplementary Fig. 9e). As expected, treatment with the JAK1/2 inhibitor Ruxolitinib disrupted this circuit, whereas TBK1/IKKε inhibition with MRT67307, partially inhibited downstream *CXCL10* expression (Supplementary Fig 9f–h). Finally, *MAVS* deletion also downregulated multiple cytokines/chemokines following Poly(I:C) or low dose IFNγ pulse treatment, especially when co-deleted with *STING* (Fig. 2k–m, Supplementary Fig. 9i, j), and impaired tumorigenicity in nude mice (Fig. 2n).

To determine the broader relevance of SPARCS and to begin to explore the relationship to immune contexture, we next ranked expression of a signature comprised of the 15 SPARCS-containing genes across the Cancer Genome Atlas (TCGA) (Pancan12, n=3602 tumors)[18] using single sample gene set enrichment analysis (ssGSEA)[19] (Fig. 3a and Supplementary Fig. 10 a, b). Top gene sets co-enriched with SPARCS-containing genes ($p<0.01$, FDR<0.01) included epigenetic, TNF/NF-κB, inflammation/innate immunity, and RTK/KRAS signaling (Fig. 3a and Supplementary Dataset 2), also observed in the Cancer Cell Line Encyclopedia (CCLE) (Supplementary Fig. 11a and Supplementary Dataset 2). In contrast, none of these signatures correlated with a control gene set derived by intersecting 3′ UTR antisense ERVs with H69M downregulated genes (Supplementary Fig. 11b and Supplementary Dataset 3). The SPARCS high state also co-associated with mutations on

chromosome 3p, including *PBRM1* and *SETD2*, as well as oncogenic *KRAS* in CCLE (Supplementary Fig. 12a, b and Supplementary Dataset 4).

At the gene level, SPARCS-containing gene expression correlated with markers of T cell and myeloid infiltration uniquely in TCGA (Supplementary Fig. 12c and Supplementary Dataset 2). In both CCLE and TCGA datasets SPARCS associated with expression of MHC, APOBEC, immune checkpoint, and EMT genes (Supplementary Fig. 12c, d and Supplementary Dataset 2). Expression of *EZH2*, *DNMT3A*, *SETD2* and multiple SWI/SNF genes inversely correlated with SPARCS (Supplementary Fig. 12c, d and Supplementary Dataset 2). We next intersected the top 1000 genes from TCGA and CCLE, to isolate robust cancer cell autonomous genes co-regulated with SPARCS (Fig. 3b and Supplementary Dataset 5). This identified B2M as the top ranked gene, followed by multiple MHC class 1 genes[20], cytosolic RNA sensors. and antigen processing machinery, all markers of a virally infected state (Fig. 3b and Supplementary Dataset 5). *TGFB1* and *AXL* were also top hits (Fig. 3b and Supplementary Dataset 5).

High expression of the SPARCS-containing gene signature in TCGA was enriched in distinct cancer histologies beyond SCLC, including clear cell renal (KIRC), lung adenocarcinoma (LUAD), head/neck squamous (HNSC), and glioblastoma (GBM) (Fig. 3c). SPARCS^{high} CCLE lines also included triple negative breast cancer (TNBC), and exhibited high relative expression of *AXL*, *MET*, *VIM*, *TGFB1* and *CD44*, and low *EZH2*, *SETD2* and SWI/SNF component expression (Supplementary Fig. 13a and Supplementary Dataset 6). SPARCS^{high} cell lines exhibited mesenchymal morphology and elevated AXL, MET and Vimentin relative to SPARCS^{low} cells (Fig. 3d and Supplementary Fig. 13b). Similar to the H69 model, SPARCS^{high} cells exhibited increased STING, but not MAVS levels (Fig. 3d and Supplementary Fig. 13a). IFNγ pulse treatment of SPARCS^{high} cells significantly induced *MLT1C49*, *CXCL10* and *PD-L1* expression relative to SPARCS^{low} cells, and inducible surface PD-L1 correlated with high baseline CD44 expression (Fig. 3e and Supplementary Fig. 14a).

We next used immune cell GSEA[21] to assess whether certain immune infiltrates might be associated with elevated SPARCS-containing gene expression in TCGA (Fig. 4a). Despite markers of cytotoxic T cells and an adaptive immune response (AIR), the top associated signatures were innate immune response (IIR) and myeloid derived suppressor cells (MDSC), followed by neutrophils and macrophages (Fig. 4a). Grouping of TCGA tumors into discrete SPARCS high/low categories (Supplementary Fig. 14b), confirmed robust and significant association of SPARCS^{high} tumors with these signatures (Fig. 4b, c). Consistent with T cell and myeloid cell chemotaxis, *CXCL10* and *CCL2* gene expression in primary tumors was tightly associated with the SPARCS^{high} state (Fig. 4d and Supplementary Dataset 6). Thus, myeloid cell infiltration may further contribute to an immunosuppressed microenvironment in SPARCS^{high} tumors.

Finally, we utilized *ex vivo* culture of patient-derived organotypic tumor spheroids (PDOTS) with autologous tumor infiltrating lymphocytes[22] to explore translational relevance of these findings. Using multiplexed immunofluorescence we confirmed T cell infiltration of two different *KRAS* mutant non-small lung cancer specimens (Fig. 4e), one with SPARCS^{high}

features including *SETD2* inactivation and APOBEC mutation pattern (NSCLC-1), and the other with *STK11*/*TP53* co-mutation (NSCLC-2) and T cell localization between tumor nests. IFNγ or Poly(I:C) treatment of NSCLC-1 PDOTS markedly enhanced production of multiple cytokines/chemokines, especially CXCL10, and sensitized them to *ex vivo* PD-1 blockade with nivolumab, in contrast to NSCLC-2 (Fig. 4f–h and Supplementary Fig. 14c–e). Thus, IFN signaling associated with the SPARCS^{high} state can be directly ascertained from patient samples and may promote sensitivity to PD-1 blockade.

Here we identify SPARCS as a novel subclass of ERVs silenced by EZH2 and poised to undergo positive feedback signal amplification due to antisense localization in 3′ UTRs of IFN stimulated genes. Whereas prior reports utilized DNMT inhibition to uncover ERVs more generally to induce a state of viral mimicry[11,12], our data reveal that mesenchymal tumor subpopulations with high AXL/MET expression and low EZH2 levels trigger expression of a specific set of ERVs when exposed to IFNγ, with important implications for understanding tumor heterogeneity and oncogenesis. This SPARCS high state was also associated with downregulation of multiple SWI/SNF components and enriched in RCC, potentially contributing to the immunogenicity recently reported following PBRM1 inactivation[23,24]. While SPARCS expression promotes MHC class 1 upregulation and T cell infiltration, activation of immune checkpoints and myeloid infiltration may promote tumor immune suppression, similar to a chronic virally infected state. Therapeutically, this may have important implications for drug combinations with PD-1 blockade. For example, in addition to blocking specific chromatin regulators[23–25], therapies that hyperactivate JAK signaling[26] or target TBK1[22,26] could alter SPARCS physiology to favor response.

Methods

Patients samples

SCLC and NSCLC human tumor samples were collected and analyzed according to Dana-Farber/Harvard Cancer Center IRB-approved protocols. These studies were conducted according to the Declaration of Helsinki and approved by Dana-Farber and Brigham and Women's Hospital IRBs.

Cell lines

The human SCLC cell lines NCI-H69, H69M, H69AR, NCI-H841, SHP77, NCI-H187, NCI-H345 and NCI-H524 were obtained from the laboratory of Dr. Joan Albanell and were authenticated following Short Tandem Repeat (STR) genotyping. Clear cell renal carcinoma (ccRCC) cell lines A704, A498, 786-O, 769-P and Caki-2 were obtained from the laboratory of Dr. William G. Kaelin Jr. and were authenticated following STR genotyping. HCC44 cell line was obtained from Broad Institute and was authenticated following STR genotyping. Jurkat T cells, THP-1 monocytes, NCI-H196, MDA-MB-231, HCC1143, MDA-MB-468, NCI-H522, T47D, MDA-MB-453, NCI-H1436, NCI-H2081 and 293T cells were obtained from the American Type Culture Collection (ATCC) (Rockville, MD) and used for all experiments before reaching 10 passages.

H69, H69M, H69AR, H841, SHP77, H187, H345, H524, H196, HCC44, MDA-MB-231, MDA-MB-453, MDA-MB-468, T47D, HCC1143, H522, H1436, H2081, THP-1, Jurkat and 769-P were cultured in RPMI-1640 (Thermo Fisher Scientific, #11875-119) containing 10% FBS (Gemini Bio-products, #100-106) and 1X pen-strep (Gemini Bio-products, #400-109). 786-O, A498 and 293T were maintained in Dulbecco's Modified Eagles Medium (DMEM) (Thermo Fisher Scientific, #11965-118) containing 10% FBS and 1X pen-strep. Caki-2 cells were maintained in McCoy's 5A medium (Life Technologies #16600108) supplemented with 10% FBS and 1X Penicillin-Streptomycin. A704 cell lines was maintained in Eagle's Minimum Essential Medium (EMEM) (Sigma, #M4780) supplemented with 2mM Glutamine (Life Technologies, #25030081), 1% Non Essential Amino Acids (NEAA) (Life Technologies, #11140-050), 1mM Sodium pyruvate (Life Technologies, #11360-070), 15% FBS and 1X Penicillin-Streptomycin.

Immunohistochemical staining

After deparaffinizing tissue blocks, antigen retrieval was achieved by wet autoclave (121 degrees Celsius, 15 min) in Antigen Retrieval Solution, pH 9 (Dako, S2367) for p-TBK1. In order to block endogenous peroxide enzyme, tissue sections were incubated for 30 minutes using Peroxidase-Blocking Solution (Dako, S2023). Then, to block non-specific background staining, tissue sections were incubated for 20 minutes with Protein Block (Dako, X0909) (human tissue) or Mouse on Mouse blocking reagent (Vector Laboratories, MKB-2213) (mouse tissue). Primary antibody specific for pTBK1 (Cell Signaling Technology, 5483; 1:50 dilution) was applied, and slides were incubated for 16 hours at 4°C. Visualization was achieved using EnVision™+/HRP, Rabbit (Dako, K4003) for pTBK1, followed by diaminobenzidine (Dako, K3468), and hematoxylin counterstain. Expression levels of pTBK1 were evaluated by two pathologists who were blinded to other data.

SCLC GEM model

All mouse experiments were conducted in accord with a Dana-Farber Cancer Institute Institutional Animal Care and Use Committee (IACUC) approved protocol. Primary tumor and metastasis tissue sections used in this study were from the genetically engineered mouse (GEM) model of SCLC consisting of the $Rb^{L/L}/p53^{L/L}$ allelic genotype [27]. A total number of 24 slices of 1 mm thickness were collected providing a sufficient number to cover the lung volume. Tumor volume per animal was quantified using 3D Slicer by manual quantification of at least 8 consecutive axial image sequences. MRI was performed to follow tumor volume and weights were monitored bi-weekly. Mice were euthanized and lungs and livers were perfused with 10% formalin, stored in fixative overnight, and embedded in paraffin. For further staining with hematoxylin and eosin (H%E) and antibodies, sections of 5 μm were cut.

Immunoblotting, antibodies and ELISA

Protein was isolated from cell lines and measured by BCA (Pierce Biotechnology). Protein extracts were subjected to polyacrylamide gel electrophoresis using the 4%–12% NuPAGE gel system (Invitrogen, Carlsbad, CA), transferred to PVDF (Millipore) membranes, and immunoblotted using antibodies that specifically recognize TBK1 (#3013), S172 pTBK1 (#5483), pERK1/2 (#4370), ERK1/2 (#9107), S473 pAKT (#4060), AKT (#9272), S396

pIRF3 (#4947), IRF3 (#4302), Y701 pSTAT1 (#9171), STAT1 (#9172), AXL (#8661), EZH2 (#5246), STING (#13647), MAVS (#3993), E-Cadherin (#3195), Vimentin (#5741), β-Actin (#4970), Tubulin (#2144), Lamin A/C (#2032) (Cell Signaling Technologies, Danvers, MA) and IKKε (#I4907) (Sigma-Aldrich, St. Louis, MO).

Secondary antibodies were from LICOR Biosciences (Lincoln, NE): IRDye 800CW Goat anti-Mouse IgG (H + L) (#926-32210), IRDye 800CW Goat anti-Rabbit IgG (H + L) (#926-32211). LICOR blocking buffer (#927-40000) was used to dilute primary and secondary antibodies, with the exception of phosho-specific antibodies, which were diluted in HIKARI Signal Enhancer Solutions 1 and Solution 2 (Nacalai USA, Inc. # NU00101). Imaging of blots and quantitation of bands was performed using the LICOR Odyssey system.

Proteome Profiler™ Human Cytokine Array Kit (#ARY005B) and CXCL10 ELISA (#DIP100) (R&D Systems, Minneapolis, MN), were performed according to manufacturer's instructions. For cytokine array, conditioned media (CM) from SCLC cells at basal conditions was collected after 48 and 72 hours. For CXCL10 ELISA, CM from IFN–γ pulsed cells was collected after 72 hours.

Microfluidic culture

Microfluidic device design and fabrication was performed as described [28], with modifications of device dimensions to accommodate larger volumes of media. DAX-1 3D cell culture chip (AIM Biotech, Singapore) was also used for select studies. H69, H69M and H69AR cell suspensions (2.5×10^4 cells) were pelleted and resuspended in type I rat tail collagen (Corning, Corning, NY) at a concentration of 2.5 mg/mL following addition of 10× PBS with phenol red with pH adjusted using NaOH. pH 7.0–7.5 confirmed using PANPEHA Whatman paper (Sigma-Aldrich, St. Louis, MO). The cell-collagen mixture was then injected into the center gel region of the 3D microfluidic culture device. Microfluidic culture devices were designed with a central region containing the cell-collagen mixture, surrounded by 2 media channels located on either side formed by bonding a coverslip to a patterned polydimethylsiloxane (PDMS) substrate. Collagen hydrogels containing cells were incubated 30 minutes at 37°C and then hydrated with media with or without 2.5×10^4 cells CFSE labeled Jurkat T cells and THP1 monocytes in the side media channels. Jurkat T cells or THP1 monocytes were labeled with the CFSE Cell Division Tracker Kit (BioLegend, San Diego, CA) following manufacturer's instructions. Following 48 hours of incubation, images were captured on a Nikon Eclipse 80i fluorescence microscope equipped with Z-stack (Prior) and CoolSNAP CCD camera (Roper Scientific). Image capture and analysis was performed using NIS-Elements AR software package. Whole device images were achieved by stitching in multiple captures. Cell quantitation was performed by measuring total cell area of CFSE dye.

Flow cytometry analysis and cell sorting

Cells were stained with anti–PD-L1 (Biolegend, Cat# 329717), anti-CD44 (Biolegend, Cat# 103011) or isotype IgG control antibodies (Biolegend, Cat# 400326 and Cat#400611), in PBS containing 2% FBS for analysis and cell sorting. Briefly, cells were washed and further

incubated with the indicated antibodies at 2 μg/mL. After 3 washes with PBS, cells were resuspended in PBS containing 2% FBS and analyzed on BD FACSCanto II or sorted to >95% purity using a BD FACSAria II. Levels were compared with isotype control antibodies. PD-L1 and CD44 mean fluorescence intensity (MFI) was normalized to isotype control. The data analyses were performed with FlowJo software (TreeStar).

Cytokine profiling

Multiplex assays were performed utilizing the bead-based immunoassay approach Bio-Plex Pro™ Human Cytokine 40-plex Assay (Cat# 171AK99MR2) on a Bio-plex 200 system (Cat# 171000201) (Bio-Rad Laboratories, Hercules, CA) and the Human Cytokine/ Chemokine Maganetic Bead Panel (Cat# HCYTMAG-60K-PX30) on a Luminex MAGPIX system (Merck Millipore, Billerica, MA). Conditioned media concentration levels [pg/ml] of each protein were derived from 5- parameter curve fitting models. Fold changes relative to the corresponding control were calculated and plotted as log2FC. Lower and upper limits of quantitation (LLOQ/ULOQ) were imputed from standard curves for cytokines above or below detection.

Quantitative RT-PCR

Total cellular RNA was extracted using the miRNeasy Mini Kit (Qiagen, Hilden, Germany) according to manufacturer's instructions. After extraction, 1 μg total RNA was used to generate cDNA with the SuperScript III First-Strand Synthesis SuperMix for qRT-PCR kit, which includes both oligo-dT and random primers (Thermo Fisher Scientific, Waltham, MA). Quantitative reverse transcription PCR (qRT-PCR) of the indicated genes (Supplementary Dataset 7) was performed using SYBR green PCR Master Mix (Applied Biosystems, Foster City, CA) and the Applied Biosystems 7300 Fast real-time PCR system and software. The relative expression was normalized with the expression of the housekeeping gene 36B4. The sequences of primers used have been listed in Supplementary Dataset 7.

Nuclear/cytoplasmic fractionation and DNA purification

Nuclear/cytoplasmic fractions from H69M PD-L1^{low} and H69M PD-L1^{high} cells were obtained according to the manufacturer's instructions (Nuclear/Cytosol Fractionation Kit, #K266-25, BioVision). Cleared extracts were treated with 20 mg/mL RNase A (Qiagen) for 30 minutes at 37ºC, 20 mg/mL Proteinase K (Thermo Fisher Scientific, Waltham, MA) for 1 hour at 55ºC and then extracted with phenol:chloroform (Invitrogen, Carlsbad, CA). DNA was isopropanol precipitated, washed with 70% Ethanol, air-dried and resuspended in water.

Digital droplet PCR

PCR reactions (25 μl) that comprised ddPCR™ Supermix for Probes, custom-made Taqman primer/probe mix and appropriate DNA template were prepared in a 96-well PCR plate and subsequently loaded onto the Automated Droplet Generator (Bio-Rad). After droplet generation, the new 96-well PCR plate was heat-sealed, placed on a conventional thermal cycler, and amplified to the end-point. After PCR, the 96-well PCR plate was read on the QX100 droplet reader (Bio-Rad). Analysis of the ddPCR data was performed with

QuantaSoft analysis software (Bio-Rad) that accompanied the droplet reader. The sequences of primers used have been listed in Supplementary Dataset 7.

ERV over-expression and knockdown

The 3′UTR TRIM22 region including the antisense MLT1C49 ERV was amplified with PCR from H69M cells RNA and cloned into pLX_307 vector. H69M PD-L1^{low} cells were transfected by nucleofection (Amaxa™ 4D-Nucleofector X Unit) according to the manufacturer's instructions (Lonza, Basel, Switzerland). RNA was isolated after 24 hours and conditioned media after 72 hours post-nucleofection with this construct versus pLX 307-GFP. 293T cells, which lack STING, were transduced with these same constructs using X-treme Gene 9 (Roche, Basel, Switzerland) according to the manufacturer's instructions, followed by isolation of both RNA and conditioned media after 72 hours to maximize sensitivity.

For knockdown experiments, H69M PD-L1^{high} cells were transfected with a scrambled negative control siRNA or two siRNAs targeting MLT1C49 (each 40nM) using Lipofectamine RNAiMAX Reagent (Thermo Fisher Scientific, Waltham, MA). RNA was isolated after 72h post-transfection to ensure knockdown.

CRISPR-Cas9 gene editing and lentiviral infection

Oligonucleotides coding for guide RNAs that target STING and MAVS genes were chosen from the Avana library and the Brunello library [29]. A non-targeting sgRNA from the Gecko library v2 was used as a dummy sgRNA for control [30]. Lenti CRISPRv2 vectors were cloned as previously described [30,31]. sgRNA target sequences are described on Supplementary Dataset 7.

293T cells were transduced with lentiCRISPRv2 using X-treme Gene 9 (Roche, Basel, Switzerland) according to the manufacturer's instructions. On day 2, target cells were seeded, and allowed to adhere overnight. On day 3 the supernatant of transduced 293T cells was collected and added to the target cells through a 0.45 μm filter. Supernatant from transduced 293T cells was again collected and added to target cells on day 4. On day 5, puromycin or blasticidin was added to select infected cells (for four days).

Compounds and treatments

Recombinant human IFN-γ (#285-IF) IFN-α (#11100-1) and IFN-β (#8499-IF) proteins were purchased from R&D Systems (Minneapolis, MN) and reconstituted in sterile, deionized water. MRT67307 and Ruxolitinib were synthesized and purchased from Shanghai Haoyuan Chemexpress Co. Both drugs were reconstituted at 10 mM in DMSO and stored at −20ºC. GSK126 (#S7061) was purchased from Selleck chemicals (Houston, TX) and reconstituted at 5 mM in DMSO and stored at −20ºC.

For IFN pulse experiments, cells were pulsed 10 minutes with IFN–γ (200 ng/mL or 10 ng/mL), IFN-α (10 000 U/mL) or IFN-β (10 000 U/mL), extensively washed, and chased in fresh media for an additional 24, 48 or 72 hours. To test drug effects on gene expression or

protein secretion, IFN–γ pulsed H69AR cells were treated with DMSO, 1μM MRT67307 or 100 nM Ruxolitinib for 24, 48 and 72 hours.

For EZH2 inhibition experiments, H69 cells were treated with 5 μM GSK126 for 6 days. Drug was replenished every 3 days with both suspension and adherent cells carried each time. After the GSK126 treatment period, equal numbers of DMSO-treated and GSK126-treated cells were exposed to either H_2O or 200 ng/mL IFN-γ for 24 hours before harvesting of RNA or conditioned media (CM).

dsRNA enrichment

For dsRNA enrichment, RNA was first treated or not for 30 min with 50 μg/ml RNase A (Qiagen, Hilden, Germany) in high-salt concentration (NaCl, 0.35 M) to prevent dsRNA degradation. After treatment, RNase A was removed by ethanol precipitation and the product was resuspended in sterile water. Next, RNase A-treated RNA was immunoprecipitated (IP) using the J2 dsRNA-specific antibody (English and Scientific Consulting Kft, Szirák, Hungary). In brief, the product of 9 μg of RNase A-treated RNA was incubated in binding buffer (150 mM NaCl, 50 mM TRIS pH8.0, 1 mM EDTA, 1% NP-40) with 5 μg of J2 antibody rotating overnight at 4°C. J2-bound dsRNA was incubated in biding buffer with 25 μL of Dynabeads Protein G (Thermo Fisher Scientific, Waltham, MA) for 4 hours at 4°C, followed by 5 washes in cold binding buffer. RNA was then extracted with TRIzol Reagent and expression levels of indicated genes were analyzed by qRT-PCR.

Enrichment of dsRNA over ssRNA was then calculated by normalizing the delta Ct of ERVs (dsRNA) against beta-actin (ssRNA).

First strand cDNA synthesis and strand specific PCR for detection of sense and antisense ERV transcripts using TASA-TD methodology

Components from the SuperScript III First-Strand Synthesis System for RT-PCR (Thermo Fisher Scientific, Waltham, MA) were adapted to perform reverse transcription with RNA from H69AR previously pulsed with IFN–γ 10 minutes. For first strand cDNA synthesis 400 ng RNA was used for β-actin, MLT1C49, MLT1A and MLT1J. 1μM of a gene specific primer ligated to a TAG-sequence not specific for the human genome (GSP sense/antisense (RT) TAG) was implemented in the reaction. RNA and primers were preheated at 65°C for 5min. For the total reaction: the GSP-TAG, 0.5mM dNTP, 5mM MgCl2, 10mM DTT, 40U RNaseOUT, 100U SuperScriptIII® RT and 240ng Actinomycin D (Sigma-Aldrich, St. Louis, MO) were added with the RNA for a 20μl reaction. Synthesis was performed at 50°C for 50 min and terminated at 85°C for 5 min. RT with extremely low intrinsic RNase H activity (for cleavage of RNA from RNA/DNA duplexes) and Actinomycin D was added to prevent second strand cDNA RT resulting in antisense artifacts [32]. After cDNA synthesis 2U recombinant RNase H was added to each reaction and incubated 20 min at 37°C. Finally, the first strand cDNA mix was ethanol precipitated and resuspended in 10 μl sterile water. Afterwards gene and strand specific qRT-PCR was performed using SYBR green PCR Master Mix. To amplify sense cDNA and antisense cDNA a TAG-primer and GSP sense-primer and a TAG-primer and GSP antisense-primer were used, respectively. We performed sense and antisense specific qRT-PCR using both sense and antisense cDNA of beta-actin as

an internal negative control that was previously demonstrated to have no antisense transcript [33]. The sequences of primers used have been listed in Supplementary Dataset 7.

Poly(I:C) treatment

For Poly(I:C) dsRNA treatment experiments, H69ARsgCTRL and H69ARsgMAVS cells were plated in RPMI media, transfected with 0.5 μg/mL Poly(I:C) HMW (InvivoGen, Sand Diego, CA) using XtremeGene HP transfection reagent (Sigma-Aldrich, St. Louis, MO) and cultured for 72 hours. On day 3 after transfection, conditioned media was recovered and CXCL10 protein expression was quantified using Human CXCL10/IP-10 Quantikine ELISA kit (R&D Systems, Minneapolis, MN). RNA was extracted and expression levels of relevant genes were analyzed by qRT-PCR.

Xenograft studies

H69AR xenograft model was established by subcutaneous (s.c.) injection of 2.5×10^5 sgCTRL or sgMAVS-H69AR cells in matrigel (Corning, Corning, NY) into the flank of nude mice (Charles River Laboratories, Wilmington, MA). Tumor volume was determined from caliper measurements of tumor length (L) and width (W) according to the formula $L \times W^2/2$. Both tumor size and body weight were measured three times per week.

Multiplexed Immunofluorescence

Multiplex Immunofluorescent staining was performed overnight for approximately 12 hours on BOND RX fully automated stainers (Leica Biosystems) as previously described [34]. Briefly, tissue sections of 5-μm thick FFPE were baked for 3 hours at 60°C before loading into the BOND RX. Slides were deparaffinized (BOND DeWax Solution, Leica Biosystems) and rehydrated with series of graded ethanol to deionized water. Antigen retrieval was performed in BOND Epitope Retrieval Solution 1 (ER1, Leica Biosystems) at pH 6 for 10 minutes at 98°C. Deparaffinization, rehydration and antigen retrieval were all preprogrammed and executed by the BOND RX. Next, slides were serially stained with primary antibodies, such as anti-CD8 (clone C8/144B; DAKO, dilution 1:5000). Incubation time per primary antibody was 40 minutes. Subsequently, anti-rabbit Polymeric Horseradish Peroxidase (Poly-HRP, BOND Polymer Refine Detection Kit, Leica Biosystems) was applied as a secondary label with an incubation time of 10 minutes. Signal for antibody complexes was labeled and visualized by their corresponding Opal Fluorophore Reagents (PerkinElmer) by incubating the slides for 5 minutes. The same process was repeated for the following antibodies / fluorescent dyes. Slides were air dried, mounted with Prolong Diamond Anti-fade mounting medium (#P36965, Life Technologies) and stored in a light-proof box at 4 °C prior to imaging. The target antigens, antibody clones, and dilutions for markers included in this report and details of controls are listed in Supplementary Table 1.

Image acquisition and analysis—Image acquisition was performed using the Mantra multispectral imaging platform (Vectra 3, PerkinElmer, Hopkinton, MA) as previously described [34]. Areas with non-tumor or residual normal tissue (i.e. residual lymph node) were excluded from the analysis. Representative regions of interest were chosen by the pathologist, and 5–7 fields of view (FOVs) were acquired at 20× resolution as multispectral

images. Image Analysis was performed using the Inform 2.3 Image Analysis Software (PerkinElmer, Hopkinton, MA).

Ex vivo culture of patient-derived organotypic tumor spheroids (PDOTS)

PDOTS from human NSCLC resection specimens were generating according to our recent publication[22]. Briefly, fresh tumor specimens were minced and resuspended in media with collagenase type IV (Life Technologies, Carlsbad, CA). After digestion, samples were strained over 100 μm filter and 40 μm filters to generate S1 (>100 μm), S2 (40–100 μm), and S3 (<40 μm) spheroid fractions. S2 spheroid fraction was pelleted and resuspended in type I rat tail collagen (Corning, Corning, NY) at a concentration of 2.5 mg/mL. The spheroid-collagen mixture was then injected into the center gel region of the 3D microfluidic culture device. Collagen hydrogels containing PDOTS were hydrated with media and treated with anti-PD-1 (Nivolumab, 100 μg/mL), IFNγ (200 ng/mL), Poly (I:C) (0.5 μg/mL) or combination (Nivolumab + IFNγ, Nivolumab + Poly (I:C)). The number of Live/Dead cells in each treatment condition was determined by Trypan Blue Exclusion method and plotted as percentage of viability. Nivolumab (Opdivo; Bristol-Myers Squibb) was obtained from the DFCI pharmacy.

OncoPanel assay

Somatic mutations, copy number variations and structural variants in parental H69 cells and H69M-PD-L1^{low}/H69M-PD-L1^{high} subpopulations were evaluated by performing the OncoPanel assay from the Center for Advanced Molecular Diagnostics from Brighman and Women's Hospital.

This OncoPanel assay surveys exonic DNA sequences of 300 cancer genes and 113 introns across 35 genes for rearrangement detection. DNA was isolated from cell lines and analyzed by massively parallel sequencing using a solution-phase Agilent SureSelect hybrid capture kit and an Illumina HiSeq 2500 sequencer.

The 300 genes are listed in Supplementary Dataset 8.

Genomic analysis and SPARCS gene set derivation

The H69 vs H69M expression microarray data analyzed in this study were obtained from the publicly available dataset GSE45120[9]. The list of 452 top genes upregulated and downregulated in H69M versus H69 is available in Supplementary Dataset 1.

ChIP-seq data for STAT1 and IRF1 data on CD14+ monocytes were retrieved from GEO database (GSE43036). Replicates data for each ChIP were aggregated into a single wiggle file and visualized in IGV genome browser at the locus of TRIM22 gene[35].

For SPARCS gene set derivation, genomic coordinates of all 3′UTR from NCBI RefSeq transcripts were intersected with all repeat elements that are 50bp or longer and have its family name containing a string 'ERV' from UCSC Repeat Masker. Those 5880 3′UTRs that overlap with any ERVs were collapsed to the gene level (Supplementary Dataset 1). Those 1,080 unique genes were further used to find overlaps with differentially expressed gene from an analysis comparing H69M vs H69. Of 452 significantly upregulated genes

(adjP<1E–4 and logFC>2) in H69M, 22 genes were found overlapped (Supplementary Dataset 1). From this list of 22 overlapping genes, we manually curated them using a UCSC genome browser (https://genome.ucsc.edu). Of the 22 ERVs, 15 of these were encoded in antisense orientation which were chose for further studies.

As we identified only 86 genes at the same threshold, the same number of genes (452) most significantly downregulated genes at logFC<1 were used to find overlaps with the genes containing ERV in its 3′ UTR (25 genes) (Supplementary Dataset 1).

SPARCS gene set enrichment analysis

The resulting list of SPARCS genes were used to perform ssGSEA analysis[36] of 585 carcinoma samples across CCLE (www.broadinstitute.org/CCLE) or 3219 samples from TCGA[18] RNAseq datasets. In brief, in ssGSEA, gene expression values are first rank-normalized ranked by their absolute expression, followed by calculation of an enrichment score (ES) of individual samples derived by evaluating the differences in the Empirical Cumulative Distribution Functions (ECDF) of the genes in the gene set (in this case the SPARCS gene set) relative to the remaining genes. A positive ES denotes significant overlap of the gene set with groups of genes at the top of the ranked list, while a negative ES denotes a significant overlap of the signature gene set with groups of genes at the bottom of the ranked list. These resulting ssGSEA scores for individual samples across CCLE or TCGA datasets were then sorted from highest to lowest and used to identify top genomic features associated with respective datasets. These included genes, mutations/copy number variations and pathways (MsigDB database). To quantify the degree of association, an information-theoretic measure of Information Coefficient (IC)[19] was calculated and an empirical permutation test for statistical significance calculations. The top 1000 genomic features significantly associated with the SPARCS signature are depicted in the heatmap.

ATAC-sequencing and analysis

We performed ATAC sequencing on H69 and H69AR cells according to [37]. Briefly, we sorted 40–50,000 cells per biological replicate, which were then washed once in cold PBS and lysed in 50μL cold lysis buffer (10 mM Tris-HCl, pH 7.4, 10 mM NaCl, 3 mM MgCl2, 0.1% IGEPAL CA-630). Lysed nuclei were incubated in Tn5 transposition reaction mix and purified using MinElute Reaction Cleanup kit (Qiagen). ATAC-seq fragments from one set of replicates for H69 and H69AR cells were size selected for fragments between 115 and 600 bp using Pippin Prep 2% Agarose Gel Cassettes and the Pippin Prep DNA Size Selection System (Sage Science). Post size-selection, ATAC libraries were amplified and Nextera sequencing primers ligated using Polymerase Chain Reaction (PCR). Finally, PCR primers were removed using Agencourt AMPure XP bead cleanup (Beckman Coulter/Agencourt) and library quality was verified using a Tapestation machine. High quality ‘multiplexed’ DNA libraries were sequenced on the Illumina HiSeq2000.

The ends of the paired-end fragments are used as cut sites and enriched peaks were called with MACS2 with following parameters (--nomodel --extsize 200 --shift -100 -g hs -B --nolambda). For IGV visualization, shifted bedGraph were converted to wig files at 10bp resolution and normalized to read counts by wigmath tool of JavaGenomic toolkit.

Statistical analyses

All graphs depict mean ± s.e.m unless otherwise indicated. Tests for differences between two groups were performed using two-tailed unpaired Student's *t*-test or Mann-Whitney's two-tailed test, as specified in the figure legends. Two-way ANOVA was performed where applicable using the Sidak *post hoc* test. P values were considered significant if less than 0.05. Asterisks used to indicate significance correspond with: *p<0.05, **p<0.005, ***p<0.001. GraphPad Prism7 was used for statistical analysis of experiments, data processing and presentation.

Data Availability

Expression Arrays Data from H69 and H69M cells are available at the Gene Expression Omnibus (GEO) under accession number GSE45120[9]. ChIP-seq data for STAT1 and IRF1 data on CD14+ monocytes are available at GEO database under accession number GSE43036[35]. Raw data for Figure 1j, Figures 3a–c, Figures 4a–d and Supplementary Figures 10–14 can be accessed in Supplementary Dataset 1–6.

Supplementary Material

Refer to Web version on PubMed Central for supplementary material.

Acknowledgments

We thank Joan Albanell, Ana Rovira and Edurne Arriola (Hospital del Mar Medical Research Institute, Barcelona, Spain) for providing human SCLC cell lines and the H69/H69M cell model. We also thank William G. Kaelin Jr. (Dana-Farber Cancer Institute, Boston, MA) for providing human ccRCC cell lines.

This work was supported by NCI-R01 CA190394-02 and NIH-U01 CA2143A1-01 (D.A.B.), the Gloria T. Maheu, Steven J. Schaubert, and Heerwagen Family Funds for Lung Cancer Research, (D.A.B.), the Rising Tide Foundation (D.A.B.), NIH/NCI P01CA120964 (K.K.W.), 5R01CA163896-04 (K.K.W), 5R01CA140594-07 (K.K.W), 5R01CA122794-10 (K.K.W), 5R01CA166480-04 (K.K.W), the Gross-Loh Family Fund for Lung Cancer Research (K.K.W), Susan Spooner Family Lung Cancer Research Fund at Dana-Farber Cancer Institute (K.K.W). Additional funding provided by NIH grants P01 CA114046, P01 CA025874, P30 CA010815, and R01 CA047159 and by the Dr. Miriam and Sheldon G. Adelson Medical Research Foundation and the Melanoma Research Foundation. The support for Shared Resources used in this study was provided by Cancer Center Support Grant (CCSG) CA010815 (to The Wistar Institute). Additional support from a Stand Up To Cancer-American Cancer Society Lung Cancer Dream Team Translational Research Grant (SU2CAACR-DT1715). Stand Up to Cancer is a program of the Entertainment Industry Foundation. Research grants are administered by the American Association for Cancer Research, the Scientific Partner of SU2C. Rohit Thummalapalli is a Howard Hughes Medical Institute Medical Research Fellow.

References

1. Hanahan D, Weinberg RA. Hallmarks of cancer: the next generation. Cell. 2011; 144:646–674. DOI: 10.1016/j.cell.2011.02.013 [PubMed: 21376230]
2. Marusyk A, et al. Non-cell-autonomous driving of tumour growth supports sub-clonal heterogeneity. Nature. 2014; 514:54–58. DOI: 10.1038/nature13556 [PubMed: 25079331]
3. Junttila MR, de Sauvage FJ. Influence of tumour micro-environment heterogeneity on therapeutic response. Nature. 2013; 501:346–354. DOI: 10.1038/nature12626 [PubMed: 24048067]
4. Tabassum DP, Polyak K. Tumorigenesis: it takes a village. Nat Rev Cancer. 2015; 15:473–483. DOI: 10.1038/nrc3971 [PubMed: 26156638]
5. Konieczkowski DJ, et al. A melanoma cell state distinction influences sensitivity to MAPK pathway inhibitors. Cancer Discov. 2014; 4:816–827. DOI: 10.1158/2159-8290.CD-13-0424 [PubMed: 24771846]

6. Tirosh I, et al. Dissecting the multicellular ecosystem of metastatic melanoma by single-cell RNA-seq. Science. 2016; 352:189–196. DOI: 10.1126/science.aad0501 [PubMed: 27124452]
7. Wu X, et al. AXL kinase as a novel target for cancer therapy. Oncotarget. 2014; 5:9546–9563. DOI: 10.18632/oncotarget.2542 [PubMed: 25337673]
8. Hata AN, et al. Tumor cells can follow distinct evolutionary paths to become resistant to epidermal growth factor receptor inhibition. Nat Med. 2016; 22:262–269. DOI: 10.1038/nm.4040 [PubMed: 26828195]
9. Canadas I, et al. Targeting epithelial-to-mesenchymal transition with Met inhibitors reverts chemoresistance in small cell lung cancer. Clin Cancer Res. 2014; 20:938–950. DOI: 10.1158/1078-0432.CCR-13-1330 [PubMed: 24284055]
10. Calbo J, et al. A functional role for tumor cell heterogeneity in a mouse model of small cell lung cancer. Cancer Cell. 2011; 19:244–256. DOI: 10.1016/j.ccr.2010.12.021 [PubMed: 21316603]
11. Chiappinelli KB, et al. Inhibiting DNA Methylation Causes an Interferon Response in Cancer via dsRNA Including Endogenous Retroviruses. Cell. 2015; 162:974–986. DOI: 10.1016/j.cell.2015.07.011 [PubMed: 26317466]
12. Roulois D, et al. DNA-Demethylating Agents Target Colorectal Cancer Cells by Inducing Viral Mimicry by Endogenous Transcripts. Cell. 2015; 162:961–973. DOI: 10.1016/j.cell.2015.07.056 [PubMed: 26317465]
13. Chuong EB, Elde NC, Feschotte C. Regulatory evolution of innate immunity through co-option of endogenous retroviruses. Science. 2016; 351:1083–1087. DOI: 10.1126/science.aad5497 [PubMed: 26941318]
14. Rouillard AD, et al. The harmonizome: a collection of processed datasets gathered to serve and mine knowledge about genes and proteins. Database (Oxford). 2016; 2016
15. Gao D, et al. Cyclic GMP-AMP synthase is an innate immune sensor of HIV and other retroviruses. Science. 2013; 341:903–906. DOI: 10.1126/science.1240933 [PubMed: 23929945]
16. Poirier JT, et al. DNA methylation in small cell lung cancer defines distinct disease subtypes and correlates with high expression of EZH2. Oncogene. 2015; 34:5869–5878. DOI: 10.1038/onc.2015.38 [PubMed: 25746006]
17. Henke C, et al. Selective expression of sense and antisense transcripts of the sushi-ichi-related retrotransposon--derived family during mouse placentogenesis. Retrovirology. 2015; 12:9. [PubMed: 25888968]
18. Hoadley KA, et al. Multiplatform analysis of 12 cancer types reveals molecular classification within and across tissues of origin. Cell. 2014; 158:929–944. DOI: 10.1016/j.cell.2014.06.049 [PubMed: 25109877]
19. Kim JW, et al. Characterizing genomic alterations in cancer by complementary functional associations. Nat Biotechnol. 2016; 34:539–546. DOI: 10.1038/nbt.3527 [PubMed: 27088724]
20. Rhodes DA, Reith W, Trowsdale J. Regulation of Immunity by Butyrophilins. Annu Rev Immunol. 2016; 34:151–172. DOI: 10.1146/annurev-immunol-041015-055435 [PubMed: 26772212]
21. Bindea G, et al. Spatiotemporal dynamics of intratumoral immune cells reveal the immune landscape in human cancer. Immunity. 2013; 39:782–795. DOI: 10.1016/j.immuni.2013.10.003 [PubMed: 24138885]
22. Jenkins RW, et al. Ex Vivo Profiling of PD-1 Blockade Using Organotypic Tumor Spheroids. Cancer Discov. 2017
23. Pan D, et al. A major chromatin regulator determines resistance of tumor cells to T cell-mediated killing. Science. 2018
24. Miao D, et al. Genomic correlates of response to immune checkpoint therapies in clear cell renal cell carcinoma. Science. 2018
25. Peng D, et al. Epigenetic silencing of TH1-type chemokines shapes tumour immunity and immunotherapy. Nature. 2015; 527:249–253. DOI: 10.1038/nature15520 [PubMed: 26503055]
26. Manguso RT, et al. In vivo CRISPR screening identifies Ptpn2 as a cancer immunotherapy target. Nature. 2017; 547:413–418. DOI: 10.1038/nature23270 [PubMed: 28723893]
27. Christensen CL, et al. Targeting transcriptional addictions in small cell lung cancer with a covalent CDK7 inhibitor. Cancer Cell. 2014; 26:909–922. DOI: 10.1016/j.ccell.2014.10.019 [PubMed: 25490451]

28. Aref AR, et al. Screening therapeutic EMT blocking agents in a three-dimensional microenvironment. Integr Biol (Camb). 2013; 5:381–389. DOI: 10.1039/c2ib20209c [PubMed: 23172153]

29. Doench JG, et al. Optimized sgRNA design to maximize activity and minimize off-target effects of CRISPR-Cas9. Nat Biotechnol. 2016; 34:184–191. DOI: 10.1038/nbt.3437 [PubMed: 26780180]

30. Sanjana NE, Shalem O, Zhang F. Improved vectors and genome-wide libraries for CRISPR screening. Nat Methods. 2014; 11:783–784. DOI: 10.1038/nmeth.3047 [PubMed: 25075903]

31. Shalem O, et al. Genome-scale CRISPR-Cas9 knockout screening in human cells. Science. 2014; 343:84–87. DOI: 10.1126/science.1247005 [PubMed: 24336571]

32. Perocchi F, Xu Z, Clauder-Munster S, Steinmetz LM. Antisense artifacts in transcriptome microarray experiments are resolved by actinomycin D. Nucleic Acids Res. 2007; 35:e128. [PubMed: 17897965]

33. Chen J, et al. Over 20% of human transcripts might form sense-antisense pairs. Nucleic Acids Res. 2004; 32:4812–4820. DOI: 10.1093/nar/gkh818 [PubMed: 15356298]

34. Carey CD, et al. Topological analysis reveals a PD-L1-associated microenvironmental niche for Reed-Sternberg cells in Hodgkin lymphoma. Blood. 2017; 130:2420–2430. DOI: 10.1182/blood-2017-03-770719 [PubMed: 28893733]

35. Qiao Y, et al. Synergistic activation of inflammatory cytokine genes by interferon-gamma-induced chromatin remodeling and toll-like receptor signaling. Immunity. 2013; 39:454–469. DOI: 10.1016/j.immuni.2013.08.009 [PubMed: 24012417]

36. Barbie DA, et al. Systematic RNA interference reveals that oncogenic KRAS-driven cancers require TBK1. Nature. 2009; 462:108–112. DOI: 10.1038/nature08460 [PubMed: 19847166]

37. Sen DR, et al. The epigenetic landscape of T cell exhaustion. Science. 2016; 354:1165–1169. DOI: 10.1126/science.aae0491 [PubMed: 27789799]

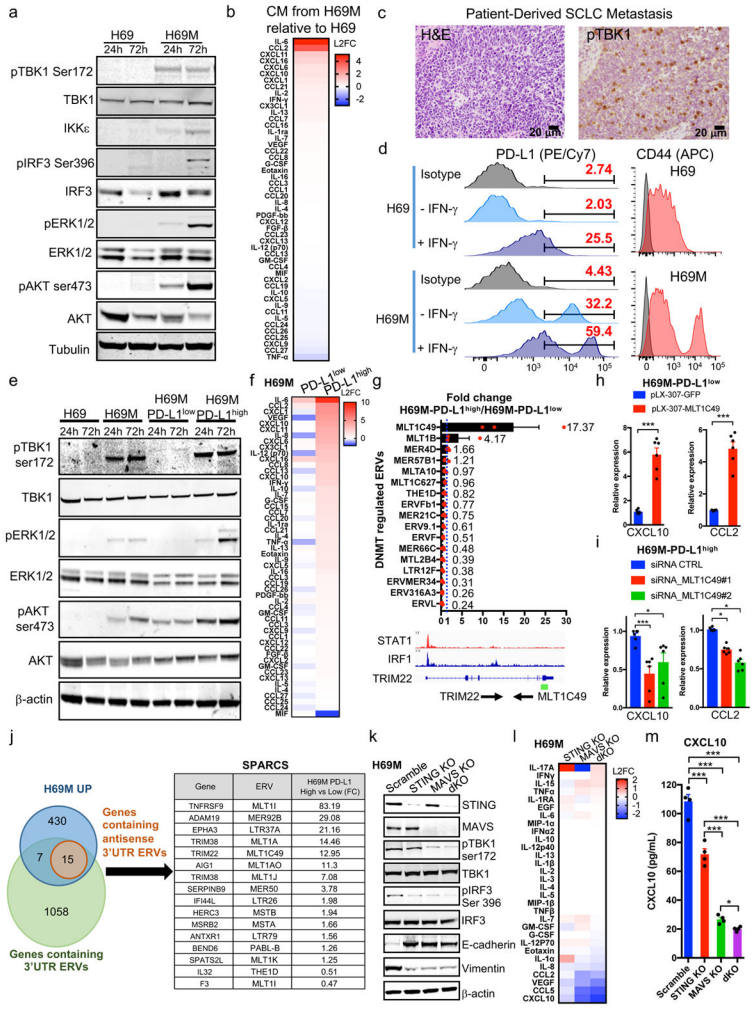

Figure 1.

Discovery of an IFN-inducible subclass of ERVs. (**a**) Immunoblot of pTBK1, TBK1, IKKε, pIRF3, pERK, ERK, pAKT, AKT and tubulin levels in H69 and H69M cells after 24 or 72 h culture. (**b**) Log-2 fold change cytokine/chemokine differences between H69M/H69 CM. (**c**) H&E and pTBK1 IHC of a patient-derived SCLC brain metastasis. Scale bar indicates 20 μm. (**d**) Isotype control versus PD-L1 or CD44 surface expression on H69 and H69M cells ± 200 ng/mL 24 h IFNγ stimulation (representative of n=3 biological replicates). (**e**) Immunoblot of pTBK1, TBK1, pERK, ERK, pAKT, AKT and β-actin levels in H69, H69M, H69M-PD-L1^{low}, and H69M-PD-L1^{high} cells. (**f**) Log-2 fold change cytokine/chemokines differences between H69M-PD-L1^{high} or H69M-PD-L1^{low}/H69 CM. (**g**) qRT-PCR of ERVs in H69M-PD-L1^{high} normalized to H69M-PD-L1^{low} cells. Numeric values on each bar represent the fold change in expression of a DNMT regulated ERV enriched panel[11,12] of previously published ERVs. Error bars are mean ± s.e.m of n=3 biological replicates. *TRIM22* promoter and antisense orientation of *MLT1C49* in the 3′UTR are represented below the qRT-PCR graph. (**h**) qRT-PCR of *CXCL10* and *CCL2* in H69M PD-L1^{low} cells transfected with pLX-307-GFP control or pLX_307-MLT1C49 construct for 72h. Mean ± s.e.m of n=3 biological replicates shown. (**i**) qRT-PCR of *CXCL10* and *CCL2* in H69M PD-

L1^{high} cells transfected with scrambled negative control siRNA or siRNAs specific for MLT1C49. Mean ± s.e.m of n=3 biological replicates shown. (**j**) Overlap of 3′UTR antisense ERVs with H69M upregulated genes (log-2 fold change relative to H69 >2) and table showing the fold change in expression of these genes/ERVs in H69M-PD-L1^{high} normalized to H69M-PD-L1^{low} cells. (**k**) Immunoblot of STING, MAVS, pTBK1, TBK1, pIRF3, IRF3, E-Cadherin, Vimentin and β-actin levels in H69M cells after CRISPR mediated deletion of MAVS and/or STING. (**l**) Log-2 fold change cytokine/chemokine differences in CM from H69M cells after CRISPR mediated deletion of MAVS and/or STING compared to sgCTRL (Scramble). (**m**) CXCL10 Luminex absolute levels (pg/mL) in Scramble, STING KO, MAVS KO and double KO (dKO) H69M cells. Mean ± s.e.m of n=2 biological replicates shown.

*p<0.05; **p<0.005; ***p<0.001; n.s., not significant (All *P* values were calculated using an unpaired two-tailed Student's *t* test).

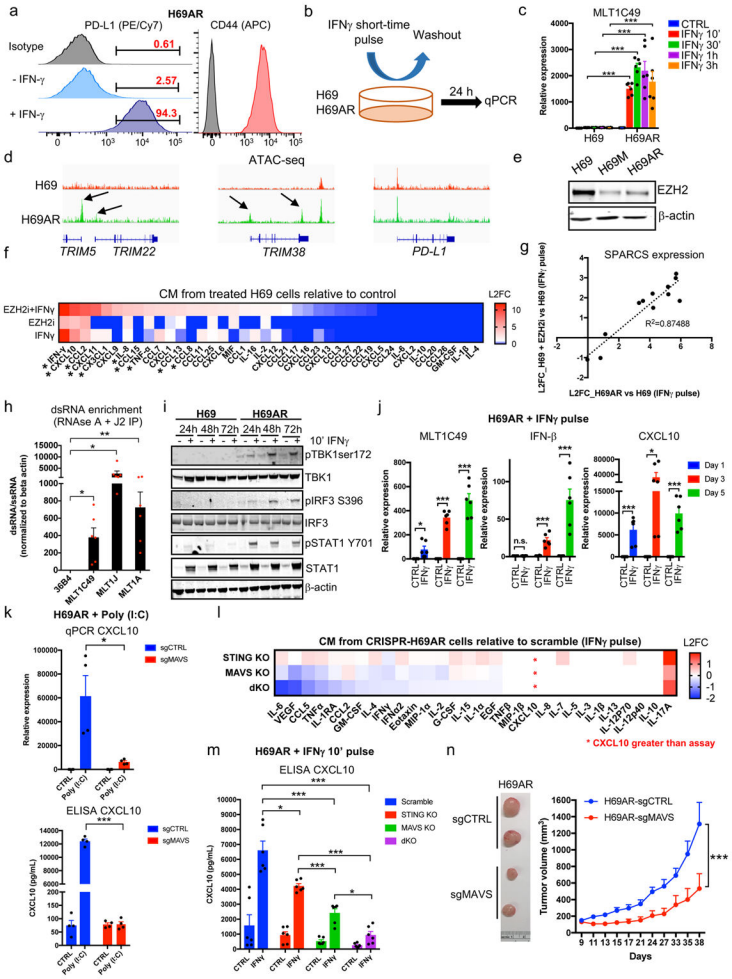

Figure 2.

SPARCS expression is inducible and triggers positive feedback amplification. (**a**) Isotype control versus PD-L1 or CD44 surface expression on H69AR cells ± 200 ng/mL 24 h IFNγ stimulation (representative of n= 3 biological replicates). (**b**) Schematic of IFNγ pulse treatment (200 ng/mL) of H69 or H69AR cells. (**c**) qRT-PCR of *MLT1C49* in H69 and H69AR cells ± 200 ng/mL IFNγ pulse – 24 h chase. Mean ± s.e.m of n=3 biological replicates shown (Two-way ANOVA; Sidak's multiple comparisons tests). (**d**) ATAC-seq insertion tracks of H69 and H69AR cells around *TRIM22*, *TRIM38* and *PD-L1*. Differentially accessible regions indicated with arrows. (**e**) Immunoblot of EZH2 and β-actin in H69, H69M and H69AR cells. (**f**) Log-2 fold change cytokine/chemokine differences between EZH2i treated H69 cells after IFNγ pulse, EZH2i treated cells, and IFNγ pulsed H69 cells relative to untreated control cells. *same as H69M-PD-L1^{high} cytokine profile in Fig. 1f. (**g**) Log-2 fold change comparison of IFNγ induced expression of SPARCS ERVs in EZH2i treated H69 cells versus H69AR cells. (**h**) qRT-PCR of *36B4* control, *MLT1C49*, *MLT1J* and *MLT1A* in H69AR cells + 10 min IFNγ pulse - 24 h chase. RNA was treated with RNase A and immunoprecipitated with anti-dsRNA J2 antibody, values normalized against beta-actin. Mean ± s.e.m of n=3 biological replicates shown (Unpaired two-tailed Student's *t* test). (**i**) Immunoblot of pTBK1, TBK1, pIRF3, IRF3, pSTAT1, STAT1 and β-

actin levels in H69 and H69AR cells ± 200 ng/mL IFNγ 10 min pulse - 24 h chase. (**j**) qRT-PCR of *MLT1C49*, *IFN-β* and *CXCL10* in H69AR cells ± 10 min IFN-γ pulse - 24 h chase. Mean ± s.e.m of n=3 biological replicates shown (Unpaired two-tailed Student's *t* test). (**k**) qRT-PCR and ELISA of CXCL10 in sgCTRL and sgMAVS-H69AR cells 72 h following Poly(I:C) transfection. Mean ± s.e.m of n=2 biological replicates shown (Unpaired two-tailed Student's *t* test). (**l**) Log-2 fold change cytokine/chemokine differences in CM between CRISPR-H69AR cells after 10 min IFNγ 10 ng/mL pulse relative to sgCTRL cells (Scramble). (**m**) CXCL10 ELISA in Scramble, STING KO, MAVS KO and dKO H69AR CM following 10 min IFNγ 10 ng/mL pulse and chase for 3 days. Mean ± s.e.m of n=3 biological replicates shown (Unpaired two-tailed Student's *t* test). (**n**) Photograph of representative excised tumors from sgCTRL and sgMAVS H69AR cells and tumor volumes measurements after 38 days of injection. Each data point represents mean ± s.e.m. tumor volumes (n=6 in sgCTRL group and n=6 in sgMAVS group; Two-way ANOVA; Sidak's multiple comparisons tests).

*p<0.05; **p<0.005; ***p<0.001; n.s., not significant.

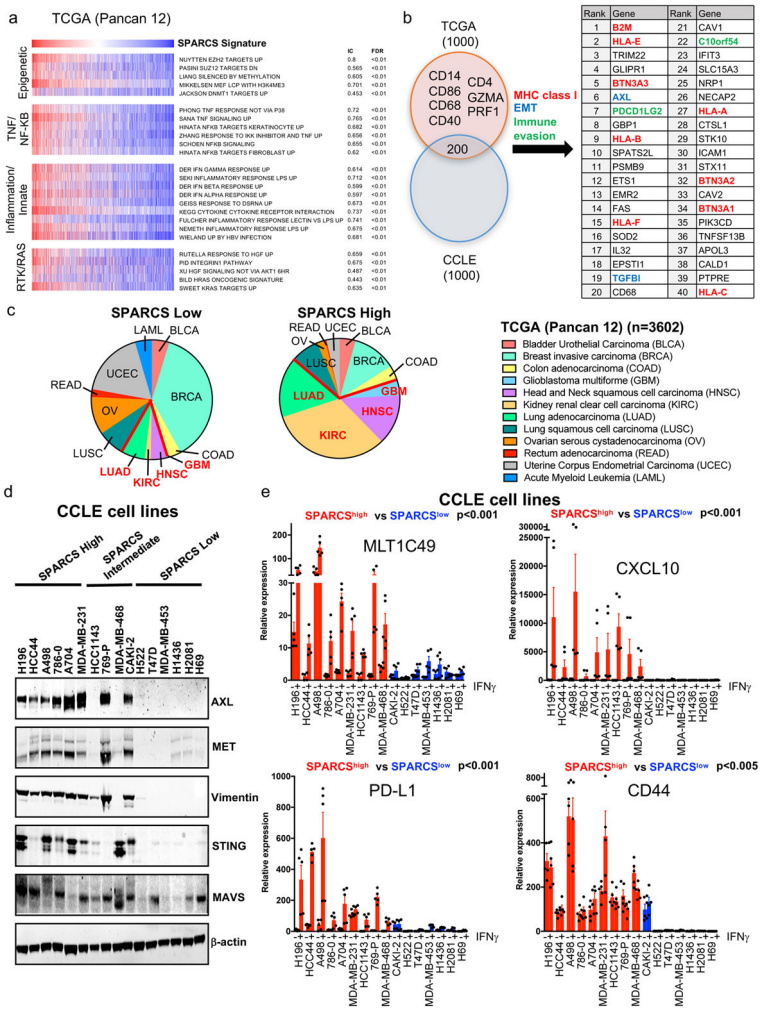

Figure 3.

Expression of SPARCS-containing genes across cancers. (**a**) ssGSEA of SPARCS-gene containing signature across TCGA (n=3602 tumors) and significantly associated gene sets grouped based on biological annotations. IC = information coefficient. FDR = false discovery rate. (**b**) Intersection of top 1000 genes co-regulated with SPARCS-containing gene signature in TCGA and CCLE datasets. MHC class I pathway genes in top 40 highlighted in red, EMT related genes in blue and immune evasion markers in green. (**c**) Distribution of high versus low SPARCS-containing gene expression by TCGA cancer histology. (**d**) Immunoblot of AXL, MET, Vimentin, STING, MAVS and β-actin levels in cell lines with high, intermediate, or low SPARCS gene signature expression after 72 h culture. (**e**) qRT-PCR of *MLT1C49, CXCL10, PD-L1* and *CD44* in $SPARCS^{high}$ and $SPARCS^{low}$ cell lines ± IFNγ 10 min pulse - 24 h chase. p values indicated for comparison of $SPARCS^{high}$ versus $SPARCS^{low}$ groups. Mean ± s.e.m of n=2 biological replicates shown (Two-tailed Mann-Whitney *U* test).

*p<0.05; **p<0.005; ***p<0.001; n.s., not significant.

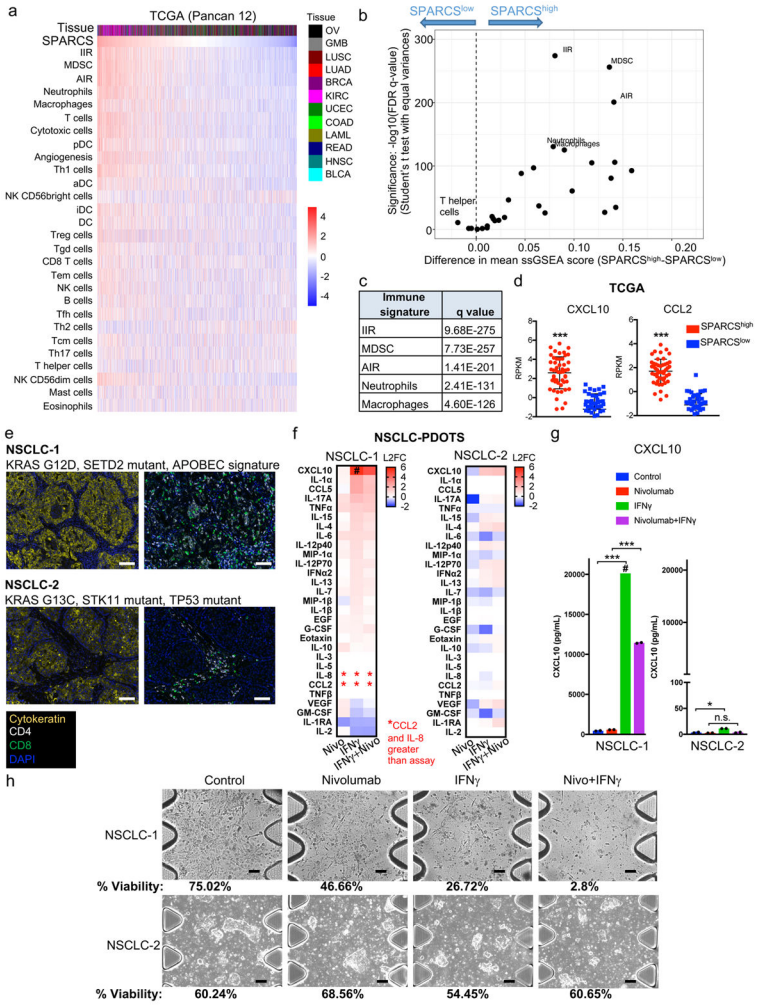

Figure 4.

SPARCS-containing gene expression is associated with adaptive and immune suppressive signatures. (**a**) ssGSEA of immune signatures in SPARCS^{high} and SPARCS^{low} primary tumors across TCGA (n=3602 tumors) and ranked based on q value significance. (**b**) Scatterplot representing difference in SPARCS^{high} vs SPARCS^{low} tumors of ssGSEA of immune signatures. $-\log_{10}$(FDR q-value) for a Student's t test with equal variances for enrichment of ssGSEA of immune signatures in SPARCS^{high} vs SPARCS^{low} tumors shown on the y-axis. Signatures more highly represented in SPARCS^{high} tumors shown on right, versus SPARCS^{low} tumors shown on left. (**c**) q value significances of ssGSEA of immune signatures in SPARCS^{high} vs SPARCS^{low} tumors across TCGA. (**d**) TCGA RPKM values of *CXCL10* and *CCL2* in primary tumors grouped in SPARCS^{high} (n=50) and SPARCS^{low} (n=50) tumors. (**e**) Multiplexed immunofluorescence staining of cytokeratin, CD8 and CD4 in *KRAS* mutant NSCLC human specimens used to generate PDOTS. Scale bar indicates 100 μm. (**f**) Cytokine/chemokine heatmap for NSCLC PDOTS treated with Nivolumab (Nivo) (100 μg/mL), IFNγ (200 ng/mL), or Nivo + IFNγ plotted as Log-2 FC relative to control. * indicates values above assay for all conditions; # indicates max CXCL10 value used to calculate Log-2FC (**g**) CXCL10 Luminex absolute levels (pg/mL). Mean ± s.e.m of

duplicate samples shown. # indicates max CXCL10 values. (**h**) Phase contrast images and viability quantification analysis of NSCLC PDOTS performed on Day 6 following treatment with Nivolumab (100 μg/mL), IFNγ (200 ng/mL), or Nivo + IFNγ. Scale bar indicates 100 μm.

*p<0.05; **p<0.005; ***p<0.001; n.s., not significant (All *P* values were calculated using an unpaired two-tailed Student's *t* test).